This manuscript has been published in the Journal of the mechanical behavior of biomedical materials, 2015 Sep 12;54:33-47. doi: 10.1016/j.jmbbm.2015.09.003.

Title: Nanoscopic dynamic mechanical analysis of resin-infiltrated dentine, under *in vitro* chewing and bruxism events.

Short title: Nano-DMA and sealing capability of dentine interfaces

Authors: Manuel Toledano[1*], Estrella Osorio[1], Inmaculada Cabello[1], Fátima S. Aguilera[1], Modesto T. López-López[2], Manuel Toledano-Osorio[1], Raquel Osorio[1].

Institution: [1]University of Granada, Faculty of Dentistry, Dental Materials Section.

Address: [1]University of Granada, Faculty of Dentistry, Dental Materials Section
Colegio Máximo de Cartuja s/n
18071 – Granada - Spain.
[2] University of Granada, Faculty of Science, Applied Physics Department
Fuente Nueva s/n
18071 – Granada - Spain.

*Corresponding author: Prof. Manuel Toledano
University of Granada, Faculty of Dentistry
Dental Materials Section
Colegio Máximo de Cartuja s/n
18071 – Granada - Spain.
Tel.: +34-958243788
Fax: +34-958240809
Email: toledano@ugr.es

HIGHLIGHTS

Sustained mechanical loading promotes failures at the resin-dentine interface.

Higher viscoelastic properties of tubular dentine concentrate stress at the interface.

Load cycling in sine or square wave promote healing at the resin-dentine interface.

ABSTRACT

The aim of this study was to evaluate the induced changes in mechanical behavior and bonding capability of resin-infiltrated dentine interfaces, after application of mechanical stimuli. Dentine surfaces were subjected to partial demineralisation through 37% phosphoric acid etching followed by the application of an etch-and-rinse dentine adhesive, Single Bond (3M/ESPE). Bonded interfaces were stored in simulated body fluid during 24 h, and then tested or submitted to the mechanical loading challenge. Different loading waveforms were applied: No cycling (I), 24 h cycled in sine (II) or square (III) waves, sustained loading held for 24 h (IV) or sustained loading held for 72 h (V). Microtensile bond strength (MTBS) was assessed for the different groups. Debonded dentine surfaces were studied by field emission scanning electron microscopy (FESEM). At the resin-dentine interface, both the hybrid layer (HL) and the bottom of the hybrid layer (BHL), and both peritubular and intertubular were evaluated using a nanoindenter in scanning mode. The load and displacement responses were used to perform the nano-Dynamic Mechanical analysis and to estimate the complex and storage modulus. Dye assisted Confocal Microscopy Evaluation was used to assess sealing ability. Load cycling increased the percentage of adhesive failures in all groups. Specimens load cycled in held 24 h attained the highest complex and storage moduli at HL and BHL. The storage modulus was maximum in specimens load cycled in held 24 h at peritubular dentine, and the lowest values were attained at intertubular dentine. The storage modulus increased in all mechanical tests, at peritubular dentine. An absence of micropermeability and nanoleakage after loading in sine and square waveforms were encountered. Porosity of the resin-dentine interface was observed when specimens were load cycled in held 72 h. Areas of combined sealing and permeability were discovered

at the interface of specimens load cycled in held 24h. Crack-bridging images appeared in samples load cycled with sine waveform, after FESEM examination.

Key words: DMA, sealing, load cycling, adhesives, dentine.

1. INTRODUCTION

Dentine occupies the majority of each tooth by both weight and volume. Its structure is composed of about 50 vol% mineral in the form of a sub-micrometer to nanometer-sized carbonate rich, calcium deficient apatite crystallites (~5 x 30 x 100 nm), dispersed between parallel, micrometer-sized, hypermineralised, collagen-poor, hollow cylinders, dentinal tubules, containing peritubular dentine. Each tubule lumen is surrounded by a peritubular cuff, which consists of a hyper-mineralised collagen-poor region (approx. 0.5 to 1 μm in thickness) of apatite crystals (Nanci, 2008; Xu and Wang, 2012). Intertubular dentine occupies the region between the tubules and consists of an organic matrix (collagen fibrils) reinforced by nanoscopic apatite crystals similar to that of peritubular dentine (Kinney et al., 2003). The organic matter represents ~30 vol%, which is largely a felt-work of type I collagen (90%) and noncollagenous proteins (10%) such as dentine matrix protein and dentine phosphoproteins, the major portion of the noncollagenous proteins, with a potent modulating effect on biomineralisation (Marshall et al., 1997). From a microstructural perspective, the collagen fibrils in dentine serve as a scaffold for mineral crystallites that reinforce the matrix. The mineral (~5 nm thickness) is differentiated between intrafibrillar (~30%, occupying the periodically spaced N terminus of the gap zones in the collagen fibril and extend along the microfibrillar spaces within the fibril) and extrafibrillar (~70%, occupying the interstices between the fibrils) (Bertassoni et al, 2009). Collagen fibrils are generally distributed randomly in intertubular dentine but are oriented circumferentially around tubules, which are considered the most distinct feature of its microstructure. Due to the differences in composition between the peritubular and intertubular components, and striking presence of the dentine tubules in microscopic evaluations, dentine is often considered a biological composite. Approximately, 20 vol% of the dentine content is fluid (Marshall et al.,1997; Pugach et al., 2009)

Dentine poses the most common dental substrate to be used in multiple adhesive techniques for restoration (De Munck et al., 2005). 'Etch-and-rinse' adhesives represent the golden standard in adhesive dentistry and involve a separate etch-and-rinse phase before the application of the adhesive. In their most common configuration, phosphoric acid (PA) is applied to demineralise the underlying dentine (De Munck et al., 2005; Osorio et al., 2005), and then, rinsed off. The conditioning step is followed by a priming step and application of the adhesive resin. This interface has been called hybrid layer (HL), made of resin and collagen (Nakabayashi, 1992; Wang and Spencer, 2003). The ideal hybrid layer would be characterized as a three-dimensional collagen-resin biopolymer that provides both a continuous and stable link between the bulk adhesive and dentine substrate (Misra et al., 2004), but a volume of demineralised/unprotected collagen remains at the bottom of the hybrid layer (BHL). It has been shown that the intertubular dentine below the exposed-collagen zone may also experience partial demineralisation, such that in the vicinity of the interface (Misra et al., 2004). This vulnerable unsupported collagen may become the sites for collagen hydrolysis by host-derived matrix metalloproteinase (MMP) enzymes (Toledano et al., 2012).

Ideally, a restoration should not only be able to chemically bond to the tooth structure, but must also behave mechanically like tooth itself in the oral environment, especially when subjected to mastication (Angker and Swain, 2006). Teeth are continuously subjected to stresses during mastication, swallowing and parafunctional habits (Frankenberger et al., 2005). Tooth contact is not a dominant activity over a 24-hour cycle. It has been estimated that tooth contact occurs for approximately 17.5 min over a 24-hour period. Sleep bruxism related with muscle activity lasts approximately 8 min over a complete sleep period that usually remains between 7 and 9 h (Lavigne et al., 2008; Okeson et al., 1990). In general, bruxism is defined as a diurnal or nocturnal

parafunctional activity that includes clenching (continuous or sustained loading), bracing, gnashing and grinding of teeth, in other than chewing (cyclic loading) movement of mandible. The range and duration of loading and the pattern of cycling loading may be intended to include physiologically realistic patterns of chewing and clenching. Duration of the chewing cycle ranges from 0.7 to 2 s, with a contact time between 0.2 and 0.3 s. During clenching, the occlusal force was observed to be as high as 520-800 N (Noma et al, 2007). The duration of bruxism episodes varies from 2 to 375 s (Jantarat et al., 2001; Abbink et al., 1999). Chewing and occlusal trauma can affect restorative strategies involving dentine. Thereby, under masticatory and parafunctional loadings, a restoration with adequate and comparable mechanical properties to that of the adjacent tooth structure will have a longer lifetime (Angker and Swain, 2006).

Previous chemico-mechanical studies have demonstrated that *in vitro* chewing and bruxism event have promoted resin-dentine interfaces highly infiltrated with resin with no presence of exposed demineralised collagen, *i.e.,* new mineral crystals embedded within a preserved collagen network. This mineral growing correlates well with an increase in nano-hardness and Young's modulus (Toledano et al., 2015). The main components of dentine behave as an effective anisotropic composite material (Misra et al., 2005), whose function is additionally complicated by biological factors that can affect both the composition and the interactions between the components. As polymers, dentine components exhibit time-dependent behavior representative of viscoelastic media. Hence, it is of interest to examine, with nano-dynamic mechanical analysis (nano-DMA), the complex indentation modulus of the resin-dentine interface attained by using an "etch-and-rinse" dentine adhesive and *in vitro* reproduction of parafunctional habits. Indentation modulus is an important parameter extracted from

nanoindentation that should not be confused with Young's or compressive modulus. Indentation modulus of a material represents the local resistance to penetration during elastic multiaxial loading (Han et al., 2011). In dynamic measurements, an oscillatory (usually sinusoidal) deformation (or force) is superimposed to a quasistatic indentation depth (or force). Thus, the nonequilibrium response of the material is assessed by obtaining the complex dynamic indentation modulus and the phase lag between the force and the deformation. This technique has been applied to create modulus maps of biological materials and some manufactured composites, demonstrating the ability to resolve microscale mechanical property variations (Bouaita et al., 2006; Han et al., 2011). Furthermore, to establish numerical modeling of restored teeth results crucial, in order to understand load transfer within the interface, which is uniquely composed of different structures with different mechanical properties, but must act as a single mechanical unit. Occlusal loading may results in high-localized stresses at bonding interfaces, thereby potentially compromising these regions, which may produce mechanical failures or microleakage, leading to secondary or recurrent caries (Angker and Swain, 2006). Thereby, it is required the capacity to absorb shock waves and alleviate stresses, at this location. *In vitro* behavior of resin-dentine interface and underlying dentine was quantified directly, under specific loading conditions, at micron and sub-micron scale. In this investigation, nano-DMA was used to evaluate dynamic mechanical behavior of human dentine, *i.e.*, to obtain the complex indentation modulus and the phase lag between force and deformation (and from these, the storage and loss moduli) in dynamic nanoindentation experiments, for the hybrid layer, bottom of hybrid layer of resin-infiltrated dentine samples, and so adjacent intertubular and peritubular dentine. The tested null hypothesis is that there is no difference in dynamic mechanical

behavior of resin-dentine interfaces created by an etch-and-rinse adhesive after *in vitro* mechanical loading.

2. MATERIAL AND METHODS.

2.1. Specimen preparation, bonding procedures and mechanical loading

Seventy five third human molars extracted for surgical reasons were obtained within informed consent from donors (20–40 year of age), under a protocol approved by the Institution Review Board. Molars were stored at 4ºC in 0.5% chloramine T for up to 1 month before use. A flat mid-coronal dentine surface was exposed using a hard tissue microtome (Accutom-50; Struers, Copenhagem, Denmark) equipped with a slow-speed, water-cooled diamond wafering saw (330-CA RS-70300, Struers, Copenhagen, Denmark). A 180-grit silicon carbide (SiC) abrasive paper mounted on a water-cooled polishing machine (LaboPol-4, Struers, Copenhagem, Denmark) was used to produce a clinically relevant smear layer (Koibuchi et al., 2001). An etch-and-rinse adhesive system, Single Bond (SB) was tested. Employed acid-etching and adhesive's description are provided in Table 1. The bonding procedure was performed in moist dentine following the manufacturer´s instructions. A flowable resin composite (X-FlowTM, Dentsply, Caulk, UK) was placed incrementally in five 1 mm layer and light-cured with a Translux EC halogen unit (Kulzer GmbH, Bereich Dental, Wehrheim, Germany) for 40 s. The teeth were stored in simulated body fluid solution (SBF) (Osorio et al., 2014) at 37ºC for 24 h, and then tested. Half of the teeth were submitted to mechanical loading tests. The specimens were divided into five groups, based on the type of mechanical loading that was applied: 1) restored teeth stored in SBF, for 24 h (no cycling); 2) load cycling with sine waveform for 24 h (259,200 cycles, 225 N, 3 Hz,) (S-MMT-250NB; Shimadzu, Tokyo, Japan); 3) load cycling with square waveform for 24 h (6,171 cycles, 225 N, 0.072 Hz,) (S-MMT-250NB; Shimadzu, Tokyo, Japan);

4) constant load (225 N) held for 24 h (Instron 3345, Instron Corporation, Canton, MA, USA); and 5) constant load (225 N) held for 72 h (Instron 3345, Instron Corporation, Canton, MA, USA). To proceed with the mechanical loaded samples, specimens were mounted in plastic rings using dental stone. The load was applied to the flat resin composite build-ups using a 5-mm diameter spherical stainless steel plunger, while immersed in SBF and proceeded as in Toledano et al. (2014). All specimens were longitudinally sectioned in 1.5-mm slabs from the central part of the specimen and polished through SiC abrasive paper from 800 up to 4.000-grit with a final polishing procedure performed with diamond pastes (Buehler-MetaDi, Buehler Ltd Illinois, USA), through 1μm down to 0.25μm. The specimens were treated in ultrasonic bath (Model QS3, Ultrawave Ltd, Cardiff, UK) containing deionised water [pH 7.4] for 5 min at each polishing step.

2.2. **Nano-DMA analysis and Atomic Force Microscopy analysis (AFM) imaging.**

Property mappings were conducted using a Hysitron Ti 950 nanoindenter (Hysitron, Inc., Minneapolis, MN) equipped with nano-DMA III, a commercial nano-DMA package. The nanoindenter tip was calibrated against a fused quartz sample using a quasistatic force setpoint of 2μN to maintain contact between the tip and the sample surface. A dynamic (oscillatory) force of 2 μN was superimposed on the quasistatic signal at a frequency of 200 Hz. Based on a calibration-reduced modulus value of 69.6 GPa for the fused quartz, the best-fit spherical radius approximation for tip was found to be 85 nm, for the selected nano-DMA scanning parameters. Modulus mapping of our samples was conducted by imposing a quasistatic force setpoint, F_q=2 μN, to which we superimposed an sinusoidal force of amplitude F_A=0.10 μN and frequency f=100 Hz. The resulting displacement (deformation) at the site of indentation was monitored as a function of time. Data from regions approximately 50x50 μm in size were collected

using a scanning frequency of 0.2 Hz. Each scan resulted in a 256 x 256 pixel data array. Specimens were scanned in the hydrated condition by the application of a layer of ethylene glycol over the specimen surface to prevent water evaporation during the analysis.

Under steady conditions (application of a quasistatic force) the indentation modulus of the tested sample, E, can be obtained by application of different models that relate the indentation force, F, and depth, D (Han et al., 2011). Most of these theories assume proportionality between the force and the indentation modulus:

$$F = g(D)E \Rightarrow E = \frac{F}{g(D)}. \qquad (1)$$

Where $g(D)$ is a function on the indentation depth, which depends on the geometry of the probe of the indenter. For example, for a spherical probe, the Hertzian contact theory predicts (Han et al., 2011; Hert, 1881):

$$g(D) = \frac{4R^{1/2}D^{3/2}}{3\left(1-\nu^2\right)}. \qquad (2)$$

In this equation R is the radius of the spherical probe and ν is the Poisson's ratio of the tested sample.

As mentioned above, in nano-DMA experiments an oscillatory force is superimposed to a quasistatic force:

$$F = F_q + F_A \sin\left(2\pi ft\right), \qquad (3)$$

with t being the time. Under this imposed force, the indentation depth takes the following form:

$$D = D_q + D_A \sin\left(2\pi ft - \delta\right). \qquad (4)$$

This means that the indentation depth also oscillates around a quasistatic value, with the same frequency that the oscillating force and delayed by a phase lag δ. In the limit of $F_A << F_q$ we can expand equation (1) to a first order Taylor approximation, to obtain:

$$F_q + F_A \sin(2\pi ft) = g(D_q)E + g'(D_q)|E^*|D_A \sin(2\pi ft - \delta). \qquad (5)$$

In this equation, g' is the first derivative of g, and E^* is the complex dynamic indentation modulus. Now, we can equal the time-dependent terms and change the time origin, to write:

$$F_A \sin(2\pi ft + \delta) = g'(D_q)|E^*|D_A \sin(2\pi ft) \qquad (6)$$

We can now decompose the oscillating force into two terms, the in-phase term, F′, and the out-of-phase term, F′′ (Macosko, 1994):

$$\begin{aligned} &F_A \sin(2\pi ft + \delta) = F_A \cos\delta \sin(2\pi ft) + F_A \sin\delta \cos(2\pi ft) = \\ &= F_A' \sin(2\pi ft) + F_A'' \cos(2\pi ft) = F' + F'' \end{aligned} \qquad (7)$$

Then, from this decomposition we can extract two dynamics moduli:

$$E' = |E^*|\cos\delta = \frac{F_A \cos\delta}{g'(D_q)D_A} = \frac{F_A'}{g'(D_q)D_A}, \qquad (8)$$

which is the in-phase or storage (elastic) modulus.

$$E'' = |E^*|\sin\delta = \frac{F_A \sin\delta}{g'(D_q)D_A} = \frac{F_A''}{g'(D_q)D_A}, \qquad (9)$$

which is the out-of-phase or loss (viscous) modulus. Note the position of the phase lag, δ, in these equations.

During the indentation mode, single indents were introduced on either hybrid layer or bottom of hybrid layer, and either the intertubular dentine or the peritubular cuff, in the vicinity of the interface. In this mode of evaluation the tip geometry and corresponding

contact area was determined using the conventional approach with a fused silica standard sample (Oliver and Pharr, 1992). For intertubular dentine, discrete indentations were made in locations that were at least 3 μm from a peritubular cuff or previous indents. For the peritubular cuffs, only single indentations were performed on a cuff due to the limited cuff thickness.

An atomic force microscope (AFM Nanoscope V, Digital Instruments, Veeco Metrology group, Santa Barbara, CA, USA) equipped with a Triboscope indentor system (Hysitron Inc., Minneapolis, MN) was employed in this study for topography mappings. The imaging process was undertaken inside a wet cell in a fully hydrated state, using the tapping mode, with a calibrated vertical-engaged piezo-scanner (Digital Instrument, Santa Barbara, CA, USA). A 10-nm-radius silicon nitride tip (Veeco) was attached to the end of an oscillating cantilever that came into intermittent contact with the surface at the lowest point of the oscillation. Changes in vertical position of the AFM tip at resonance frequencies near 330 kHz provided the height of the images registered as bright and dark regions. 50 x 50 μm digital images were recorded from each resin-dentine interface, with a slow scan rate (0.1 Hz).

2.3. Microtensile Bond Strength.

After the different procedures, 30 teeth (two from each group) were sectioned into serial slabs, and further into beams with cross-sectioned areas of 1 mm^2. Specimens were attached to a modified Bencor Multi-T testing apparatus (Danville Engineering Co., Danville, CA) with a cyanoacrylate adhesive (Zapit/Dental Venture of America Inc., Corona, CA, USA) and stressed to failure in tension (Instron 4411 /Instron Inc., Canton, MA, USA) at a crosshead speed of 0.5 mm/min. The cross-sectional area at the site of failure of the fractured specimens was measured to the nearest 0.01mm with a pair of digital calipers (Sylvac Ultra-Call III, Fowler Co Inc., Newton, Mass, USA). Bond

strength values were calculated in MPa. Fractured specimens were examined with a stereomicroscope (Olympus SZ-CTV, Olympus, Tokyo, Japan) at 40x magnification to determine the mode of failure. Failure modes were classified as adhesive or mixed. Representative specimens of each group were maintained for 48 h in a desiccator (Sample Dry Keeper Simulate Corp., Japan), mounted on aluminum stubs with carbon cement and sputter-coated with pure gold by means of a sputter-coating Unit E500 (Polaron Equipment Ltd., Watford, England). Prepared specimens were observed with a scanning electron microscopy (SEM) (HRSEM Gemini, Carl Zeiss, Oberkochen, Germany) at an accelerating voltage of 20 kV, in order to observe the morphology of the debonded interfaces. MTBS values were analyzed by two-way ANOVA (independent factors are mechanical loading and adhesive type) and Student Newman Keuls multiple comparisons tests. For all tests, statistical significance was set at a = 0.05.

2.4. ***Dye assisted Confocal Microscopy Evaluation (CLSM).***

Thirty further dentine-bonded specimens were prepared as described in 2.1. Previous to adhesive application, bond resin was doped with 0.05 wt% Rhodamine-B (Rh-B: Sigma-Aldrich ChemieGmbh, Riedstr, Germany). Half of the specimens were submitted to the different mechanical loading tests (as described in previous section). Afterwards, teeth were divided into two groups:1) the pulpal chamber was filled with 1 wt% aqueous/ethanol fluorescein (Sigma-Aldrich Chemie Gmbh, Riedstr, Germany) for 3 h (Sauro et al., 2012), in 15 specimens (three molars per group), and 2) immersed in 0.5 wt% xylenol orange solution (XO: Sigma-Aldrich ChemieGmbh, Riedstr, Germany), excited at 514-nm for 24 h, at 37 ºC (pH 7.2). Xo is a calcium-chelator fluorophore commonly used in hard tissues remineralisation studies, due to its ability to form complexes with divalent calcium ions (Profeta el al., 2013). Specimens were

copiously rinsed with water and treated in an ultrasonic water bath for 2 min. Then, they were cut in resin-dentine slabs and polished using ascending grit SiC abrasive papers (#1200 to #4000) on a water-cooled polishing device (Buehler-MetaDi, Buehler Ltd. Lake Bluff, IL, USA). A final ultrasonic treatment (5 min) concluded the specimen preparation. Analysis of bonded interfaces were performed by dye assisted confocal microscopy evaluation (CLSM), and attained by using a confocal laser scanning microscope (SP5 Leica, Heidelberg, Germany) equipped with a 20x, 40x and 60x oil immersion lenses. The fluorescein was excited at 488-nm, while the ultramorphology evaluation (resin-diffusion) was executed using a 568-nm krypton (rhodamine excitation) laser. CLSM images were obtained with a 1 μm z-step to optically section the specimens to a depth up to 12-10 μm below the surface. The z-axis scans of the interface surface were arbitrarily pseudo-coloured by the same operator for better exposure and compiled into single projections using the Leica image-processing software SP2 (Leica, Heidelberg, Germany). Five optical images were randomly captured from each resin-dentine interface. Micrographs representing the most common features of permeability observed along the bonded interfaces were captured (Toledano et al., 2013; Profeta et al., 2012). Fluorescences were or not separated into spectral regions, allowing that the operator has a full control of the region of the light spectrum directed to each channel.

3. RESULTS AND DISCUSSION

Our findings suggest that discrepancies between viscoelastic properties of both hybrid layer and bottom of hybrid layer respect to the tubular dentine system, after mechanical stimuli, create failures at the interface which damage the integrity of the resin-dentine interface. Load cycling did not affect bond strength at any group, but contributed to increase the percentage of adhesive over mixed failures (Table 2). The

effect of load cycling in dentine bonding efficacy, throughout dental literature, results controversial; in general terms, a decrease in bonding efficacy after using Single Bond has been previously reported after mechanical loading (Toledano et al., 2006). It was pointed out that fatigue stress (Nikaido et al., 2002) produces a failure mostly at the top or beneath the HL where demineralised collagen fibrils were exposed and the adhesive failed to envelop the collagen network properly (Toledano et al., 2006; Prati et al., 1999). The increase in the percentage of adhesive failures may be interpreted as a result after the strengthening of the resin-dentine interface from remineralisation (Toledano et al., 2015).

The work performed by the probe of the nanoindentator in the adhesive interface is divided into two parts that follow two different routes: *i)* elastic energy, which is stored in the material and returned to the probe within each oscillating cycle; *ii)* viscous energy, which is dissipated as heat (Gong and Guan, 2003; Espino et al, 2014). Storage and viscous moduli account respectively for the energy stored and dissipated. These visco-elastic moduli are calculated from the stiffness and damping moduli of the sample. They are obtained by subtracting the stiffness and damping moduli of the sensor from the measured stiffness and damping moduli, which are the combined values of the sensor and the sample (Hayot et al., 2012). In stiff (mainly elastic) samples such as dentine, the substrate absorbs stress after loading, but there will be negligible dissipation of energy by heat and, thus, the damping modulus of the sample is very close to zero (Chuang et al., 2015; Lakes et al., 2009). Consequently, at certain positions within our samples, the actual value of the loss modulus cannot be obtained with confidence, as the damping modulus of the sample is masked by the damping modulus of the sensor; thereby, these values are not presented in the manuscript.

How, structurally, the resin-dentine interface dissipates and stores energy is likely to be related to the stress transfer mechanism during dentine-polymer interaction. Due to the increase in mineral content at the resin-dentine interface after mechanical loading (Toledano et al., 2015) changes to the viscoelastic mechanical behavior are not unexpected. The increased mineralisation after mechanical loading (Toledano et al., 2015) was only accompanied by an augmented complex modulus, at the HL, when mechanical load was applied on held 24 h. At the bottom of hybrid layer, both intrafibrillar mineralisation (Toledano et al., 2015) and complex modulus augmented simultaneously in all groups of study (Table 3), though sustained held for 24 h attained the highest E*. The significance of this finding lies on the major resistance to deformation that is achieved at the resin-dentine interface, among all mechanically tested groups (Table 3). This greater complex modulus correlates well with greater stiffness (Ryou et al., 2013), and is in good agreement with the mean complex modulus determined from scanning-base nano-DMA obtained after using the contemporary etch-and-rinse adhesive One-Step (3.5 GPa). These data are hardly comparable since Ryou et al. (2013) promoted resin infiltration in a completely demineralised dentine substrate.

Specimens loaded in sustained held 24 h also achieved the highest elastic or storage modulus, at both HL and BHL (5.11 and 1.84 GPa, respectively) when compared with the rest of the groups (Table 3). It is the highest ability to store potential energy which is released after deformation when load is maintained constant for 24 h. At HL, unloaded samples attained 3.6 GPa of storage modulus, close to 3.4 GPa (Ryou et al., 2013) and 5GPa (Katz et al., 2001) of elastic energy stored, values that were recently reported. Dissipation of energy within the structures is of prime importance in dynamic systems (Agrawal et al., 2013) such as the oral function, where teeth and restorations require damping to absorb shock waves and alleviate stresses. Hence,

improving damping characteristics becomes imperative for enhancing their robustness thereby expanding their lifetimes. Transfer of energy during contact from the adhesive to resin-dentine interface, and from the resin-dentine interface to the underlying dentine may have implications for the viscoelastic response of the dentine-polymer complex interaction. It is noteworthy the quotient between both complex and storage moduli at the HL and BHL. When specimens were loaded in held 24 h, the complex modulus decreased ~ 1.08 fold from HL to BHL. On the contrary, the storage modulus decreased ~5.96 fold in the same trend. Low modulus regions lead to stress concentration in relatively high elastic modulus regions (Misra et al., 2004). Thereby, if the energy stored is too great, then excess energy would potentially be dissipated through cracking the tissue; *i.e.,* resin-dentine interface failure. This mechanism would be consistent with resin-dentine inter-diffusion zone breakdown, preferentially the hybrid layer, occurring through increased energy during impact loading (Espino et al., 2014). This failure coincides with the gap that was formed within the resin-dentine interface which clearly detached the hybrid layer from the bottom of the hybrid layer, though both structures became deeply remineralised (Fig 2D). These results, *i.e.*, stored energy and its ensuing dentine-polymer interaction failure coincide with and extended area of micropermeability and nanoleakage detected underneath the rhodamine B-labeled adhesive layer (Fig 3/4·IA). Fluorescein infiltrated the top of the rodhamine B-labeled hybrid layer throughout both the wall of the tubules (cylinders in yellow) and the partially porous hybrid layer (HL, in green and yellow). Multi-fluorescence examination permitted to observe overlapping between both original channels (rhodamine/red, fluoresceine/green) resulting in yellow (Pawley, 2006), showing a profuse dye signal throughout the thickness of the hybrid layer and tubules. This indicates water sorption an micropermeability within the resin tags structures that resulted damages after

cracking the resin-dentine interface, concretely the HL and its crossing resin tags (Figs 3/4·IB, 3/4·IC). The fluorescein penetration stopped several microns away from the resin-dentine interface, characterized by many wide and middle-size resin tags (Fig 3/4·IB), but achieved the damage area. Length of resin tags may have been conditioned by some new formations, non present in the unloaded specimens (Fig 3/1A), that occupy the lumen of tubules. The reason why only short resin tags could be created during this procedure is supported by the existence of the strong reflective signal from the beginning of the canaliculi, probably indicating the presence of mineral segments. This hypothesis was also validated when immersing the specimens in the xylenol orange solution (Profeta et al., 2013; Toledano et al., 2013). In general, load cycled specimens treated with XO-dye produced a clearly outlined fluorescence due to a consistent Ca-minerals deposited within the bonding interface and inside the dentinal tubules (Figs 3/2·IIA, 3/4·IIA). Nevertheless, light funneling of the tubular orifices was evident with a good penetration of the adhesive into the tubules and their lateral branches.

When specimens were load cycled in held 24 h, the complex moduli achieved at peritubular and intertubular dentine attained the highest values (68.45 and 80.62 GPa, respectively) among all tests, and it was ~2.74 and 4.72 fold higher than values attained in the unloaded groups (25 and 17 GPa, respectively). Our values of complex modulus, in the control or unloaded group are within the range previously published by Kinney et al. (1999) and Katz et al. (2001), who reported 26-30 GPa and 13-20 GPa for peritubular and intertubular dentine, respectively. In the dentine microstructure each dentine tubule is surrounded by a highly mineralised zone, ~ 1 μm thick, called the peritubular dentine (Balooch et al., 2004). Scanning of selected regions of interest enabled identification of both peritubular and intertubular dentine in the property maps,

and revealed that there is heterogeneity in the mechanical property distribution of those regions. Microstructural analysis unveils mineral deposits within the lumen of tubules, after mechanical stimulation (Figs 2·VI, 2·VII). Differences in porosity at the interface, respect to the unloaded group, which affects the permeability and fluorescein transport properties through the dentine, are specially remarkable in specimens cyclic loaded in held 24 and 72 h, may also be observed. When sustained load was applied for 72 h, a tight fluorescein sorption throughout the thickness of the HL was detected, which extended until the total adhesive thickness, but it was more concentrated in the dentine vicinity (Figs 3/5A, 3/5B). In some tubules, a discrete spectral overlap (yellow) was appreciated in the emission of profile of both dyes (red and green), indicating further pathways of water uptake, presence of micro-canals for the advance of permeability and future degradation of the dentine-polymer interaction through nanoleakage (Profeta et al., 2013; Toledano et al., 2013). This mineral depleted and non-sufficiently infiltrated etched dentine was also observable as a dentine substrate scarcely remineralised, at both intertubular and peritubular locations (Fig 2E), indicating the pathway for further degradation.

The depth of dentine demineralisation during etching clearly exacerbates the stress concentration problem within the peritubular dentine; thereby, the failure initiation point lies within the peritubular dentine (Misra et al., 2004). From the stress distribution mapped by Misra et al. (2004), it can be inferred that failure or fracture could probably initiate at three locations in the HL and the dentine: *(i)* in the adhesive tag proximal to the HL due to stress concentration, *(ii)*, close to the BHL due to high strain; and *(iii)* interface between the adhesive tag and peritubular dentine of the lumen wall due to stress concentration (Misra et al., 2005). Moreover, if the bond between the adhesive tags and peritubular dentine is imperfect permitting micro-permeability (Fig

3/5A), then the stress concentration zones are probably within the HL and BHL, where stresses will concentrate and the integrity of the resin-dentine interface will be jeopardized. Therefore, the stress concentrations at peritubular dentine are amplified for cases with lower elastic moduli at the HL or BHL, as occurs in specimens load cycled in 72 h (Fig 1/VI), where the relation between E' of HL+BHL/2 and E' of peritubular dentine was ~19.62 fold bigger (Fig 1/VB) than in samples loaded with sine or square waveforms (~10.62 and 15.35, respectively) (Table 3). Thereby, resin-dentine interfaces load cycled in sine and square waveforms produced null presence of both micropermeability and water sorption at the completely sealed interface (Figs 3/2·IA, 3/2·IIA, 3/3A), as a result of an advanced mechanism of mineral precipitation (Figs 2B, 2C), which additionally causes crystal filling of the transverse secondary tubules and restricts water and fluorescein movement. It has been stated that larger loading of dentine results in larger strain and advance remineralisation. This finding may be interpreted as resin-dentine interfaces which result highly infiltrated with resin, with no presence of exposed demineralised collagen, *i.e.,* new mineral crystals embedded within a preserved collagen network (Toledano et al., 2014). At least when load cycling was executed on dentine interfaces with sine and square waveforms, complementary use of nano-DMA and confocal microscopy demonstrate that the present biomimetic remineralisation effect which results after load cycling, is capable of achieving the nanomechanical heterogeneity present in mineralised dentine. Biomimetic remineralisation of resin-sparce regions of resin-dentine interface also protects the denuded collagen fibrils from degradation (Osorio et al., 2014) and restores the dynamic materials behavior of the mineralised tissue.

When load was not applied, the storage moduli of peritubular and intertubular dentine were 24 and 16 GPa, respectively. Balooch et al. (2004) obtained 48 and 21

GPa, respectively. More recently, Ryou et al. (2015) have obtained an overall average complex modulus of old intertubular and peritubular dentine of ~21 and 31 GPa and storage moduli values of ~20 and 30 GPa, respectively. The discrepancy between results that were obtained could be a result of, but are not limited to, age, race, location or gender of the samples, but most importantly to the fact that their measurements were performed in dry conditions (Balooch et al., 2004). The different viscoelastic properties which show both type of dentines could be a result of the high concentration of collagen fibrils in the intertubular dentine, and is an outcome of higher store potential energy available for elastic recoil (Balooch et al., 2004) at peritubular dentine (Table 3). At tubular structures, energy dissipation can occur via deformation in axial and radial directions (Agrawal et al., 2013), as validated from the FESEM images. One of the major damage mechanisms during cycling loading in a tubular system is the formation of microcracks that propagate along the tubular process, becoming unstable after exceeding a critical threshold. This culminates in fast fracture and the failure of the structural interface. It has been demonstrated that the tubular system suppress failure through crack-bridging and frictional pullout (Agrawal et al., 2013). We speculate that the dentine submitted to load cycling could make up for the formation of large cracks by nucleating minerals at micro and nano-scale damage zones. Those new mineral formations were observed, *e.g.*, in samples submitted to load cycling in sine waveform, where multiple rod-like figures were detected surrounding the intratubular crystals (Fig 2B·I), and "bridging" different layers of slipped mineralised dentine (Figs 1·VII, 2B·II, 2B·III). These mineral beams maintained anchored, *i)* directly (arrow) or indirectly (pointer) (crack-bridging) the intratubular deposits of mineral to the peritubular dentine, and *ii)* distinct mineralisation fronts at the intertubular dentine, each other (frictional pullout). Pullout of stick-slip procedures are well-known mechanisms for energy

dissipation previously studied within nanotube structures (Grimmer et al., 2009; Agrawal et al., 2013). These bridge-like structures were also observed in other locations, and have contributed to enhance the long-term behavior of composites under cyclic loading (Agrawal et al., 2013). Nevertheless, this lack of hermetic sealing, obtained from our imaging data, between both intratubular and peritubular dentine (Fig 2B·I) and between different layers of bridged remineralised dentine (Fig 2B·II) may have permitted the micropermeability which was detected beyond the mineralised tubuli, toward the resin dentine interface (Figs 3/2·IA, 3/2·IC, 3/2·IIA).

These are, to the best of our knowledge, the only available results from nano-DMA experiments on resin-dentine interfaces submitted to different pattern of *in vitro* mechanical loading. These outcomes are important, because they provide information on structure and viscoelastic changes produced at micro and nano-scale at restorative-dentine interfaces; however, additional correlation analyses of the properties of the whole interface (adhesive and intact dentine) are still needed. Hence, improving the dissipation of energy within the resin-dentine interface becomes imperative for enhancing therapy and expanding the lifetime of dental restorations. Further work is now required to determine the mechanism by which load cycling prevent mechanical-induced changes in dentine mineralisation and dentine strength. Nevertheless, our study also has several weakness; longer duration of mechanical loading, inclusion of remineralising agents and bioactive ions into the chemical formula of adhesives, effect of the temperature, and to consider other mechanical properties as compressive modulus or fracture modulus would have expanded the message of this paper, and should have been considered. These represent topics for further research. Moreover, these measurements open up the possibility of future probing of other materials-tooth

interfaces, *e.g.*, self-etching adhesives and glass-ionomer cements, as well as extending the assessments to other hard tissues as enamel, cementum and bone.

CONCLUSIONS.

The transfer of energy has implications for the viscoelastic response of the dentine-polymer complex interaction when sustained mechanical loading is applied, promoting failures at the resin-dentin interface. Higher viscoelastic properties of tubular dentin concentrate stress at the interface, where the integrity of the resin-dentin interface is jeopardized. Load cycling in sine or square wave promotes healing at the resin-dentin interface, with null presence of both micropermeability and water sorption

ACKNOWLEDGMENTS.

This work was supported by grants MINECO/FEDER MAT2014-52036-P and FIS2013-41821-R.

The authors have no financial affiliation or involvement with any commercial organisation with direct financial interest in the materials discussed in this manuscript. Any other potential conflict of interest is disclosed.

REFERENCES

Abbink, J.H., Van der Bilt, A., Bosman, F., Van der Glas, H.W., 1999. Speed-dependent control of cyclic open–close movements of the human jaw with an external force counteracting closing. J. Dent. Res. 78, 878–886.

Agrawal, R., Nieto, A., Chen, H., Mora, M., Agarwal, A., 2013. Nanoscale damping characteristics of boron nitride nanotubes and carbon nanotubes reinforced polymer composites. ACS Appl. Mater. Interfaces 27, 12052-12057.

Angker, L., Swain, M.V., 2006. Nanoindentation: Application to dental hard tissue investigations. J. Mater. Res. 21, 1893-1905.

Balooch, G., Marshall, G.W., Marshall, S.J., Warren, O.L., Asif, S.A., Balooch, M., 2004. Evaluation of a new modulus mapping technique to investigate microstructural features of human teeth. J. Biomech. 37, 1223-1232.

Bertassoni, L.E., Habelitz, S., Kinney, J.H., Marshall, S.J., Marshall, G.W. Jr., 2009. Biomechanical perspective on the remineralization of dentin. Caries Res. 43, 70-77.

Bouaita, N., Bull, S.J., Palacio, J. F., White, J.R., 2006. Dynamic nanoindentation of some polyolefins. Polym. Eng. Sci. 46, 1160-1172.

Chuang, S.F., Lin, S.Y., Wei, P.J., Han, C.F., Lin, J.F., Chang, H.C., 2015. Characterization of the elastic and viscoelastic properties of dentin by a nanoindentation creep test. J. Biomech. pii: S0021-9290(15)00050. doi:10.1016/j.jbiomech.2015.01.034.

De Munck, J., Van Landuyt, K., Peumans, M., Poitevin, A., Lambrechts, P., Braem, M., Van Meerbeek, B., 2005. A critical review of the durability of adhesion to tooth tissue:methods and results. J. Dent. Res. 84, 118-132.

Espino, D.M., Shepherd, D.E., Hukins, D.W., 2014. Viscoelastic properties of bovine knee joint articular cartilage: dependency on thickness and loading frequency. BMC Musculoskelet. Disord. 14, 15:205.

Frankenberger, R., Pashley, D.H., Reich, S.M., Lohbauer, U., Petschelt, A., Tay, F.R., 2005. Characterisation of resin-dentine interfaces by compressive cyclic loading. Biomaterials. 26, 2043-2052.

Gong, J., Guan, Z., 2003. Strength characteristics of toughened ceramics containing contact-induced small surface cracks. Mater. Sci. Eng. A344,132-139.

Grimmer, C.S., Dharan, C.K.H., 2009. High-cycle fatigue life extension of glass fiber/polymer composites with carbon nanotubes. J.Wuhan Univ Technol. Mater. Sci. Ed. 24, 167-173.

Han, L., Grodzinsky, A.J., Ortiz, C., 2011. Nanomechanics of the Cartilage Extracellular Matrix. Annu. Rev. Mater. Res. 41, 133-168.

Hayot, C.M., Forouzesh, E., Goel, A., Avramova, Z., Turner, J.A., 2012. Viscoelastic properties of cell walls of single living plant cells determined by dynamic nanoindentation. J. Exp. Bot. 63, 2525-2540.

Hertz, H., 1881. Über die Berührung fester elastischer Körpen (On the contact of rigid elastic solids). J. R. Angew. Math. 92, 156–171.

Jantarat, J., Palamara, J.E., Messer, H.H., 2001. An investigation of cuspal deformation and delayed recovery after occlusal loading. J. Dent. 29, 363-370.

Katz, J.L., Bumrerraj, S., Dreyfuss, J., Wang, Y., Spencer, P., 2001. Micromechanics of the dentin/adhesive interface. J. Biomed. Mater. Res. Appl. Biomater. 58, 366-371.

Kinney, J.H., Balooch, M., Marshall, G.W., Marshall, S.J., 1999. A micromechanics model of the elastic properties of human dentine. Arch. Oral Biol., 44, 813-822.

Kinney, JH., Marshall, SJ., Marshall, GW., 2003. The mechanical properties of human dentin: a critical review and re-evaluation of the dental literature. Crit. Rev. Oral Biol. Med. 14, 13-29.

Koibuchi, H., Yasuda, N., Nakabayashi, N., 2001. Bonding to dentin with a self-etching primer: the effect of smear layers. Dent. Mater. 17, 122-126.

Lakes, S.R., Lee, T., Bersie, A., Wang, Y.C., 2001. Extreme damping in composite materials with negative-stiffness inclusions. Nature 410, 565-567.

Lavigne, G.J., Khoury, S., Abe, S., Yamaguchi, T., Raphael, K., 2008. Bruxism physiology and pathology: an overview for clinicians. J. Oral Rehabil. 35, 476-494.

Lee, S.W., Hinsberg, W.D., Kanazawa, K.K., 2002. Determination of the viscoelastic properties of polymer films using a compensated phase-locked oscillator circuit. Anal. Chem.74, 125-131.

Macosko, C.W., 1994; Rheology: Principles, Measurements, and Applications, VCH: New York.

Marshall, G.W. Jr, Marshall, S.J., Kinney, J.H., Balooch, M., 1997. The dentin substrate: structure and properties related to bonding. J. Dent. 25, 441-458.

Misra, A., Spencer, P., Marangos, O., Wang, Y., Katz, J.L., 2004. Micromechanical analysis of dentin/adhesive interface by the finite element method. J. Biomed. Mater. Res. B Appl. Biomater. 70, 56-65.

Misra, A., Spencer, P., Marangos, O., Wang, Y., Katz, J.L., 2005. Parametric study of the effect of phase anisotropy on the micromechanical behaviour of dentin-adhesive interfaces. J. R. Soc. Interface. 22, 145-157.

Nakabayashi N., 1992. The hybrid layer: a resin-dentin composite. Proc. Finn. Dent. Soc. 88 (Suppl 1), 321-329.

Nanci, A., 2008. Ten Cate's Oral Histology: Development, Structure and Function. St. Louis, Mosby.

Nikaido, T., Kunzelmann, K.H., Chen, H., Ogata, M., Harada, N., Yamaguchi, S., Cox, C.F., Hickel, R., Tagami, J., 2002. Evaluation of thermal cycling and mechanical loading on bond strength of a self-etching primer system to dentin. Dent. Mater. 18, 269-275.

Noma N., Kakigawa H., Kozono Y., Yokota M., 2007. Cementum crack formation by repeated loading in vitro. J Periodontol. 78,764-769.

Okeson, J.P., Phillips, B.A., Berry, D.T., Cook, Y., Paesani, D., Galante, J., 1990. Nocturnal bruxing events in healthy geriatric subjects. J. Oral Rehabil. 17, 411-418.

Oliver, W.C., Pharr, G.M., 1992. An Improved Technique for Determining Hardness and Elastic-Modulus Using Load and Displacement Sensing Indentation Experiments. J. Mater. Res. 7**,** 1564-1583.

Osorio, R., Erhardt, M.C., Pimenta, L.A., Osorio, E., Toledano, M., 2005. EDTA treatment improves resin-dentin bonds' resistance to degradation. J. Dent. Res. 84, 736-740.

Osorio, R., Osorio, E., Medina-Castillo, A.L., Toledano, M., 2014. Polymer nanocarriers for dentin adhesion. J. Dent. Res. 93, 1258-1263.

Pawley, J.B., 2006. Handbook of biological confocal microscopy. Maddison, USA: Springer.

Profeta, A.C., Mannocci, F., Foxton, R., Watson, T.F., Feitosa, V.P., De Carlo, B., Mongiorgi, R., Valdré, G., Sauro, S., 2013. Experimental etch-and-rinse adhesives doped with bioactive calcium silicate-based micro-fillers to generate therapeutic resin-dentin interfaces. Dent. Mater. 29, 729-741.

Prati, C., Chersoni, S., Pashley, D.H., 1999. Effect of removal of surface collagen fibrils on resin-dentin bonding. Dent. Mater.15, 323-331.

Pugach, M.K., Strother, J., Darling, C.L., Fried, D., Gansky, S.A., Marshall, S.J., Marshall, G.W., 2009. Dentin Caries: Mineral structure, and properties. J. Dent. Res. 88, 71-76.

Ryou, H., Pashley, D.H., Tay, F.R., Arola, D., 2013. A characterization of the mechanical behavior of resin-infiltrated dentin using nanoscopic Dynamic Mechanical Analysis. Dent. Mater. 29,719-728.

Ryou, H., Romberg, E., Pashley, D.H., Tay, F.R., Arola, D., 2015. Importance of age on the dynamic mechanical behavior of intertubular and peritubular dentin. J. Mech. Behav. Biomed. Mater. 42, 229-242.

Sauro, S., Osorio, R., Watson, T.F., Toledano, M., 2012. Therapeutic effects of novel resin bonding systems containing bioactive glasses on mineral-depleted areas within the bonded-dentin interface. J. Mater. Sci. Mater. Med. 23, 1521-1532.

Toledano, M., Aguilera, F.S., Sauro, S., Cabello, I., Osorio, E., Osorio, R., 2014. Load cycling enhances bioactivity at the resin-dentin interface. Dent. Mater. 30, e169-e188.

Toledano, M., Cabello, I., Aguilera, F.S., Osorio, E., Osorio, R., 2015. Effect of in vitro chewing and bruxism events on remineralization, at the resin-dentin interface. J Biomech. 48, 14-21.

Toledano, M., Osorio, R., Albaladejo, A., Aguilera, F.S., Tay, F.R., Ferrari, M., 2006. Effect of cyclic loading on the microtensile bond strengths of total-etch and self-etch adhesives. Oper. Dent. 31, 25-32.

Toledano, M., Sauro, S., Cabello, I., Watson, T., Osorio, R., 2013. A Zn-doped etch-and-rinse adhesive may improve the mechanical properties and the integrity at the bonded-dentin interface. Dent. Mater. 29, e142-e152.

Toledano, M., Yamauti, M., Ruiz-Requena, M.E., Osorio, R., 2012. A ZnO-doped adhesive reduced collagen degradation favouring dentine remineralization. J. Dent. 40, 756-765.

Wang, Y., Spencer, P., 2003. Hybridization efficiency of the adhesive/dentin interface with wet bonding. J. Dent. Res. 82, 141-145.

Xu, C., Wang, Y., 2012. Collagen cross linking increases its biodegradation resistance in wet dentin bonding. J. Adhes. Dent. 14, 11-18.

CAPTIONS FOR FIGURES.

Figure 1: Nano-DMA and AFM analyses. Scanning mode nano-DMA analysis of the resin-dentine interface in the unloaded (no cycling) group (I), after load cycling in sine waveform (II), after load cycling in square waveform (III), after load cycling in held 24 h (IV), after load cycling in held 72 h (V). (A) Property map of the complex modulus. (B) Corresponding property map of the storage modulus. Fig 1·IVA reflects the three possible locations of failure at the resin-dentine interface of a specimen loaded in held 24 h, in the tag proximal to the hybrid layer (arrow), close to the bottom of hybrid layer (pointer), and interface between the tag and peritubular dentine (asterisk). Fig 1·VB shows the place of stress concentration at peritubular dentine when the elastic moludi at the hybrid layer and bottom of hybrid layer are low, as in specimens load cycled in held 72 h. (VI) 3-D contour map of the complex modulus (E*) distribution in a specimen submitted to constant load in held for 72 h. At the resin-dentine inter-diffusion zone, E* ranged from 3.19 (hybrid layer) to 59.51 (peritubular dentine) GPa.(VII) AFM image of the resin-dentine interface obtained after load cycling in sine. Mineralised tubular occlusion (arrows), and rod-like new minerals or "stick-slip" formations (pointers) were determined after observation. (VIII) AFM image of the resin-dentine interface obtained after load cycling in held 24 h. Resin tags (arrows) and mineral formations (pointers) occupy the lumen of tubules.

Figure 2: Field emission scanning electron microscopy images of failures after bonding and MTBS testing. (A) Unloaded (control). (B) Load cycled in sine waveforms. (C) Load cycled in square waveforms. (D) Load cycled in held 24 h waveforms. (E) Load cycled in held 72 h waveforms. (A), a mixed failure and fracture at the bottom of hybrid

layer may be observed. Collagen fibers are clearly discernible (pointers) at the peritubular (PD) and intertubular dentine (ID), and some of them appearing mineralised (asterisks). The majority of tubules are empty and open (arrow). (B), a mixed failure and a firm tubular occlusion (asterisk) was shown when the specimens were cyclic loaded in sine waveforms. This substratum resulted completely mineralised, and the mineral formations only allowed a restricted display of the tubule entrances (asterisks). Rod-like new mineral formations were observed surrounding the intratubular crystals (B·I). These mineral beams maintained directly (arrow) or indirectly (pointer) anchored the intratubular deposits of mineral to the peritubular dentine. Different layers of mineralised dentine were also anchored each other through these rod-like new formations (B·II) (faced arrows). "Stick-slip" images of remineralised dentine were also observable at the interface (B·III). (C), a mixed failure was determined when specimens were load cycled in square waveforms. Dentine (intertubular and peritubular) was strongly mineralised. Crystals precipitated in knob-like formations, at intertubular dentine (ID), where they nucleated preferentially. Clumps of precipitation of minerals, in strata (asterisk), covered the whole surface of dentine matrix, allowing the visual observation of open tubules and some collagen fibbers (arrow). Minerals also precipitated around the tubule wall, forming a collar around the narrowest ring of the tubule entrance (pointer).The typical staggered pattern of collagen fibrils due to the characteristic D- periodicity (67 nm) was visible at the fibbers which cover the entrance of the peritubular dentine (double arrow). (D), a mixed failure was shown when specimens were load cycled in held 24 h waveforms. A generalized mineral deposition was completely covering the dentine surface, though adhesive failure (double arrows), and fracture between hybrid layer and bottom of hybrid layer may be observed (faced pointers). Mineralised dentine collagen was detected forming the bottom of the hybrid

layer (asterisck), where multiple collagen fibrils appeared longitudinally mineralised (pointer). Multiple amorphous clumps of material scattered and grouped as dense network of buttons-like mineral nuclei were also exhibited. Tubules turned up totally mineral filled but without protruding from the entrance of tubules (arrow). (E), a mixed failure was shown when specimens were load cycled in held 72 h waveforms, affecting both the adhesive surface (asterisk) and the partially demineralised dentine (arrow) at the bottom of the hybrid layer. An extensive labyrinth of reticular mineral depositions, vastly inter-connected, made of resin and mineral were perceptible (pointer). Collagen fibers were clearly observed at the peritubular dentine (PD), appearing completely demineralised. The bottom of the hybrid layer exhibited tubule entrances totally visible and empty.

Figure 3: Dye assisted Confocal Microscopy Evaluation (CLSM) of resin-dentine interfaces.

3/1. CLSM images showing the interfacial characterization and micropermeability of the resin-dentine interface created using Single Bond (SB) adhesive applied on phosphoric acid-etched dentine, and obtained at 63x, with 25 μm of scale bar. Figs A and B show a generalized pattern of severe micropermeability and water sorption (arrows) at both adhesive layer (a) and dentinal tubules (t), and between dentine (d) and the adhesive layer (pointer). A porous HL and an intense nanoleakage signal from the hybrid layer (asterisk) located underneath the rhodamine B-labeled adhesive layer may be observed, in reflexion/fluorescence mode (A). In the CLSM image captured in fluorescence mode, it is possible to observe an adhesive layer characterized by the presence of many wide and long resin tags (rt) when imaged in rhodamine excitation/emission mode (B) underneath the adhesive layer, and a profuse dye sorption

throughout its thickness when imaged in fluorescein excitation/emission mode (C). Funnelling (f) of the tubular orifices is evident with good penetration of the adhesive (a) into the tubules and their lateral branches (lb). a, adhesive layer; d, dentine; f, funneling; hl, hybrid layer; lb, lateral branches; rt, resin tags; t, dentinal tubules.

3/2·I. CLSM images showing the interfacial characterization and micropermeability of the resin-dentine interface created using Single Bond (SB) adhesive applied on phosphoric acid-etched dentine, load cycled in sine waveform, and obtained at 63x-2 optical zoom, with 10 μm of scale bar. Null presence of both micropermeability and water sorption were observed when samples were imaged in reflexion/fluorescence mode (A). No signs of nanoleakage at the hybrid layer (hl) (arrow), and a strong reflective signal from the dentinal tubules (pointer) were detected, indicating the presence of multiple mineral segments (asterisk). In fluorescence mode (rhodamine excitation/emission), long and short resin tags (rt) are observed. (B). In fluorescence mode (fluoroscein excitation /emission), any water sorption within the thickness of the adhesive (a) can be seen (C), and fluoroscein concentrated below the hybrid layer at intertubular dentine (id), and within the permeable dentinal tubules. a, adhesive layer; d, dentine; rt, resin tags; t, dentinal tubules.

3/2·II. CLSM single-projection image disclosing the fluorescent calcium-chelators dye xylenol orange of the resin-dentine interface created using Single Bond (SB) adhesive applied on phosphoric acid-etched dentine, load cycled in sine waveform, and obtained at 63x-2 optical zoom, with 10 μm of scale bar, imaged in reflexion/fluorescence mode (A), rhodamine excitation/emission mode (B) and calcium-chelators dye xylenol orange only (C). A clear fluorescence signal due to consistent presence of xylenol-stained Ca-deposits within the hybrid layer (hl), walls of dentinal tubules (arrows) (dt) and resin

tags (rt) was observed. Note the presence of multiple intact resin tags (rt) imaged in Rhodamine excitation/emission mode (B). hl: hybrid layer; rt, resin tags; dt, dentinal tubules.

3/3. CLSM images showing the interfacial characterization and micropermeability of the resin-dentine interface created using Single Bond (SB) adhesive applied on phosphoric acid-etched dentine, load cycled in square waveform, and obtained at 63x-2 optical zoom, with 10 μm of scale bar. No signs of nanoleakage (pointer) and a moderate reflective signal from the demineralised dentine layer and inside the dentinal tubules (arrows), indicating the presence of mineral components, were detected when imaged in reflexion/fluorescence mode. Intertubular dentine appeared totally infiltrated (asterisk), sealing the resin-dentine interface. No further dye diffused into the adhesive layer and shorter or thinner resin tags (rt) are detected in fluorescence mode (rhodamine excitation/emission) (B). In fluorescence mode, (fluoroscein excitation /emission) both no penetration of fluoroscein throughout the dentinal tubules and water sorption within the thickness of the adhesive can be seen (C). a, adhesive layer; d, dentine; rt, resin tags; t, dentinal tubules.

3/4·I. CLSM images showing the interfacial characterization and micropermeability of the resin-dentine interface created using Single Bond (SB) adhesive applied on phosphoric acid-etched dentine, load cycled in held waveform for 24 h, and obtained at 63x-2 optical zoom, with 10 μm of scale bar. Fig A shows a generalized pattern of micropermeability and water sorption (arrows) at both intertubular dentine (id) and dentinal tubules (t) (reflexion/fluorescence). A porous and faint HL, with an intense nanoleakage signal (asterisk) located underneath the rhodamine B-labeled adhesive layer, may be observed. Dye did not diffuse to the adhesive layer, but resin-dentine interface appeared partially sealed by the adhesive approximately 5-7 μm below the

surface of dentine (pointer). Some nanoleakage signal from the hybrid layer may be observed (double arrow). In the CLSM image captured in fluorescence mode, it is possible to observe an adhesive layer characterized by the presence of many wide and middle-size resin tags (rt) when imaged in rhodamine excitation/emission mode (B) underneath the adhesive layer. A profuse dye sorption signal throughout the thickness of the hybrid layer, tubules and lateral branches (lb) was imaged in fluorescein excitation/emission mode (C). Funnelling (f) of the tubular orifices is evident with good penetration of the adhesive (a) into the tubules and their lateral branches (lb). a, adhesive layer; d, dentine; hl, hybrid layer; lb, lateral branches; rt, resin tags; t, dentinal tubules.

3/4·II. CLSM single-projection image disclosing the fluorescent calcium-chelators dye xylenol orange of the resin-dentine interface created using Single Bond (SB) adhesive applied on phosphoric acid-etched dentine, load cycled in held 24 h waveform, and obtained at 63x-2 optical zoom, with 10 μm of scale bar, imaged in reflexion/fluorescence mode (A), rhodamine excitation/emission mode (B) and calcium-chelators dye xylenol orange only (C). A moderate fluorescence signal due to consistent presence of xylenol-stained Ca-deposits within the hybrid layer (hl), dentinal tubules (dt) and resin tags (rt). Note the presence of multiple intact resin tags (rt) imaged in Rhodamine excitation/emission mode (B). hl: hybrid layer; rt, resin tags; dt, dentinal tubules.

3/5. CLSM images showing the interfacial characterization and micropermeability of the resin-dentine interface created using Single Bond (SB) adhesive applied on phosphoric acid-etched dentine, load cycled in held waveform for 72 h, and obtained at 63x-2 optical zoom, with 10 μm of scale bar. Fig A shows a sailed interface by the adhesive (a), but with a tight dye sorption throughout its thickness (asterisk). A strong

reflective signal may be described from the bottom of the hybrid layer (hl) and inside the dentinal tubules (arrows), in reflexion/fluorescence mode. The adhesive layer is characterized by the presence of wide and short (B) resin tags (rt) when imaged in fluorescence mode (rhodamine excitation/emission) and by a tight (C) dye sorption throughout the *canaliculi* lumens and conditioned dentine. In fluorescence mode (fluoroscein excitation /emission), water sorption within the thickness of the adhesive can be seen (asterisk). It is possible to observe a well marked hybrid layer. a, adhesive layer; d, dentine; hc, hybrid layer; rt, resin tags; t, dentinal tubules.

GRAPHICAL ABSTRACT

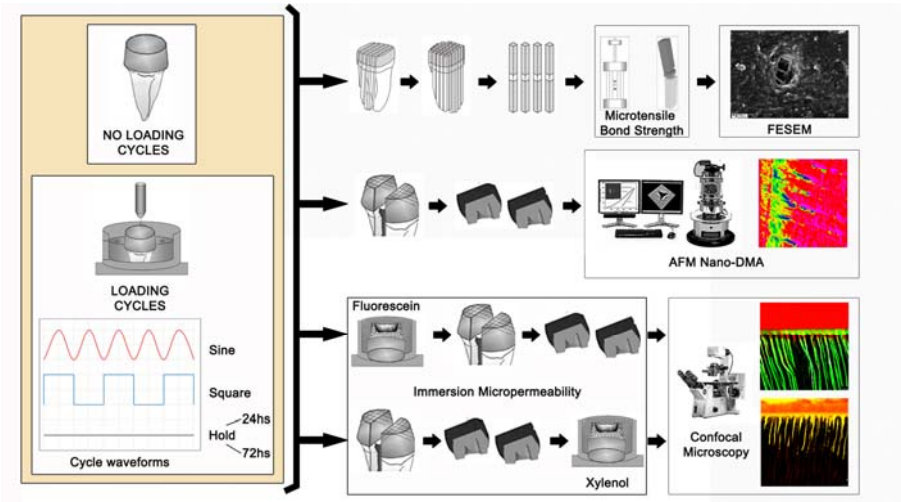

FIGURE 1 (I,II,III)

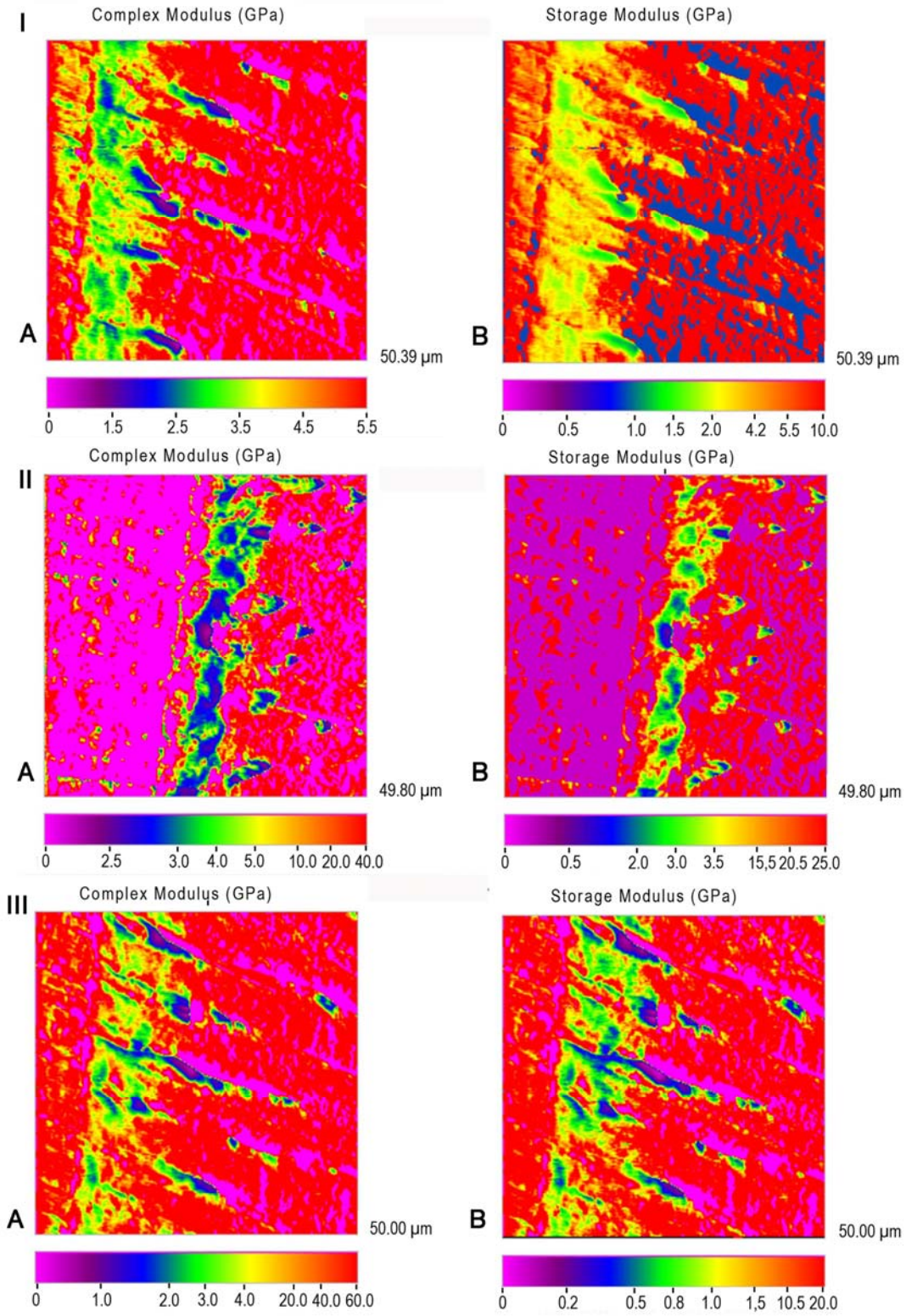

FIGURE 1 (IV,V)

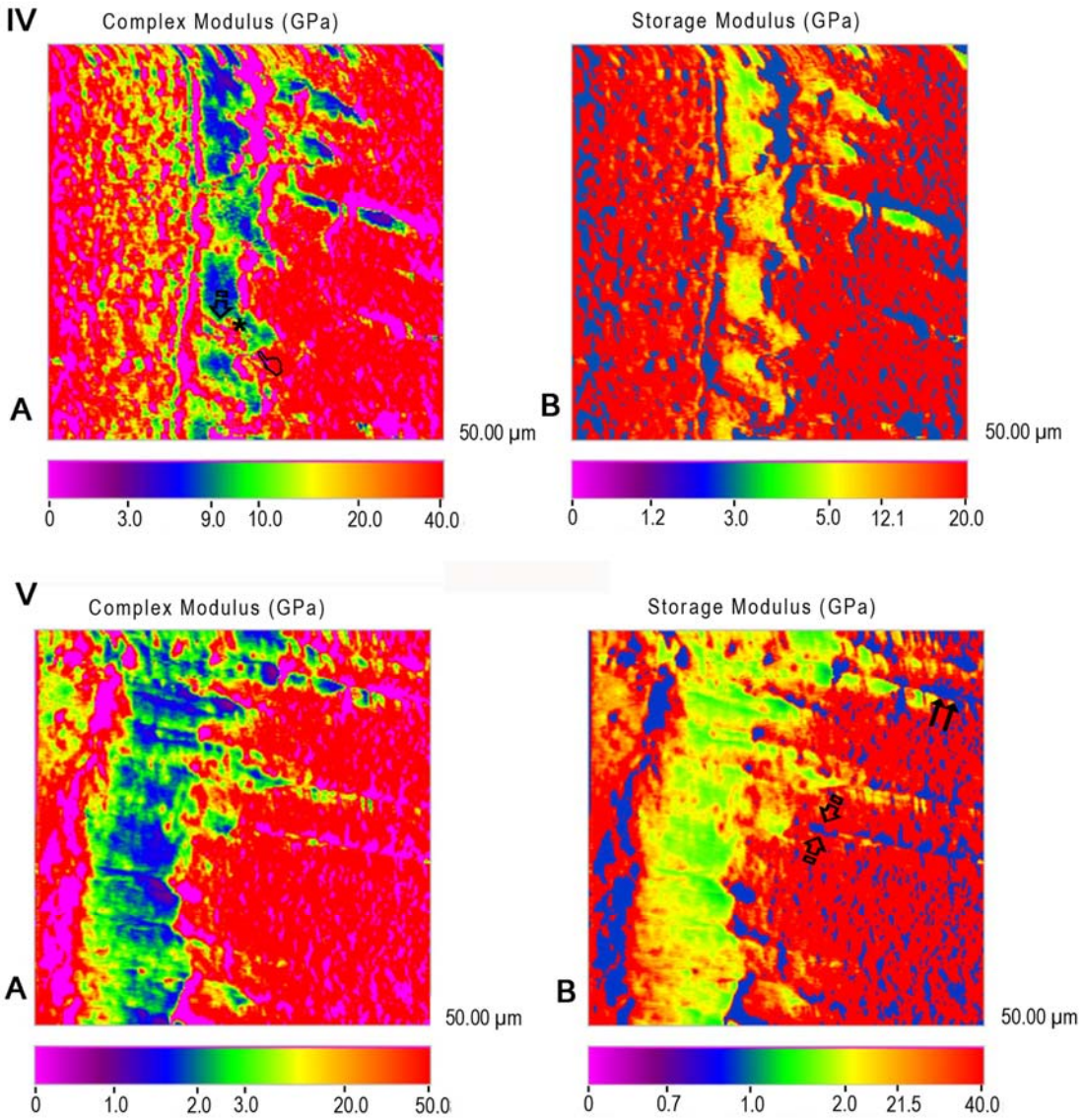
IV
Complex Modulus (GPa)
Storage Modulus (GPa)
A
B
50.00 µm
50.00 µm
0 3.0 9.0 10.0 20.0 40.0
0 1.2 3.0 5.0 12.1 20.0
V
Complex Modulus (GPa)
Storage Modulus (GPa)
A
B
50.00 µm
50.00 µm
0 1.0 2.0 3.0 20.0 50.0
0 0.7 1.0 2.0 21.5 40.0

FIGURE 1 (VI)

VI

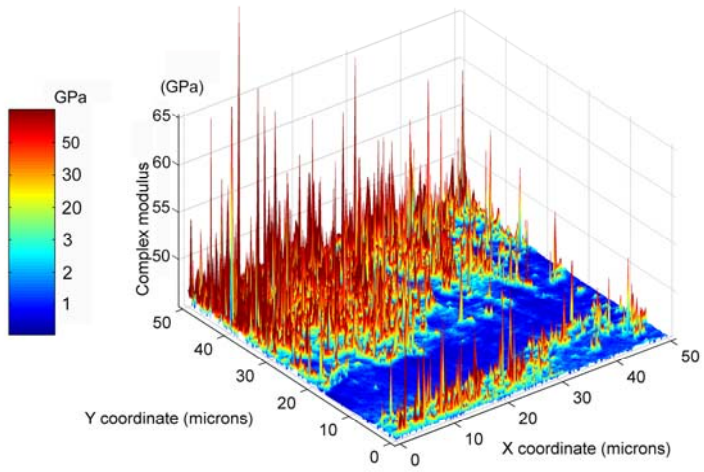

FIGURE 1 (VII)

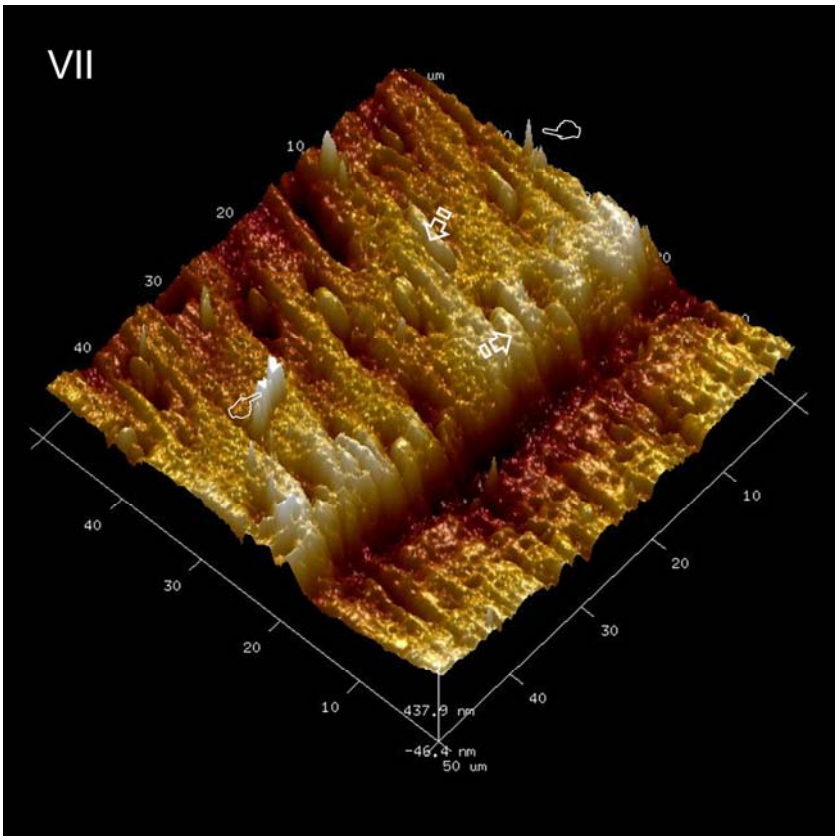

FIGURE 1 (VIII)

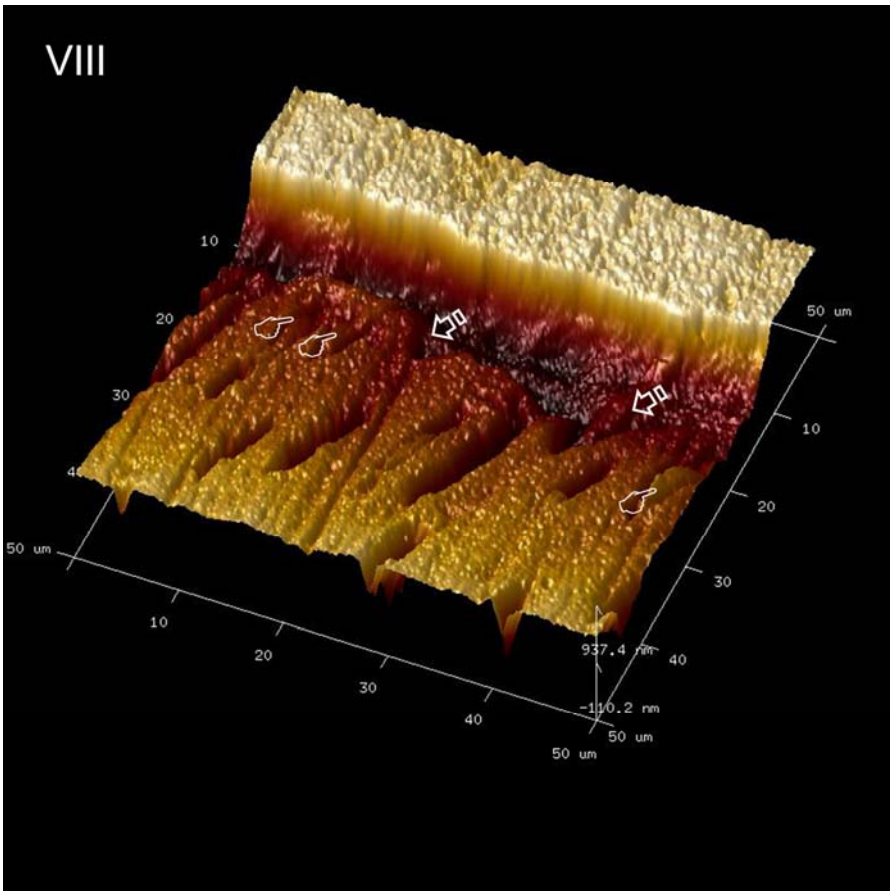

FIGURE 2

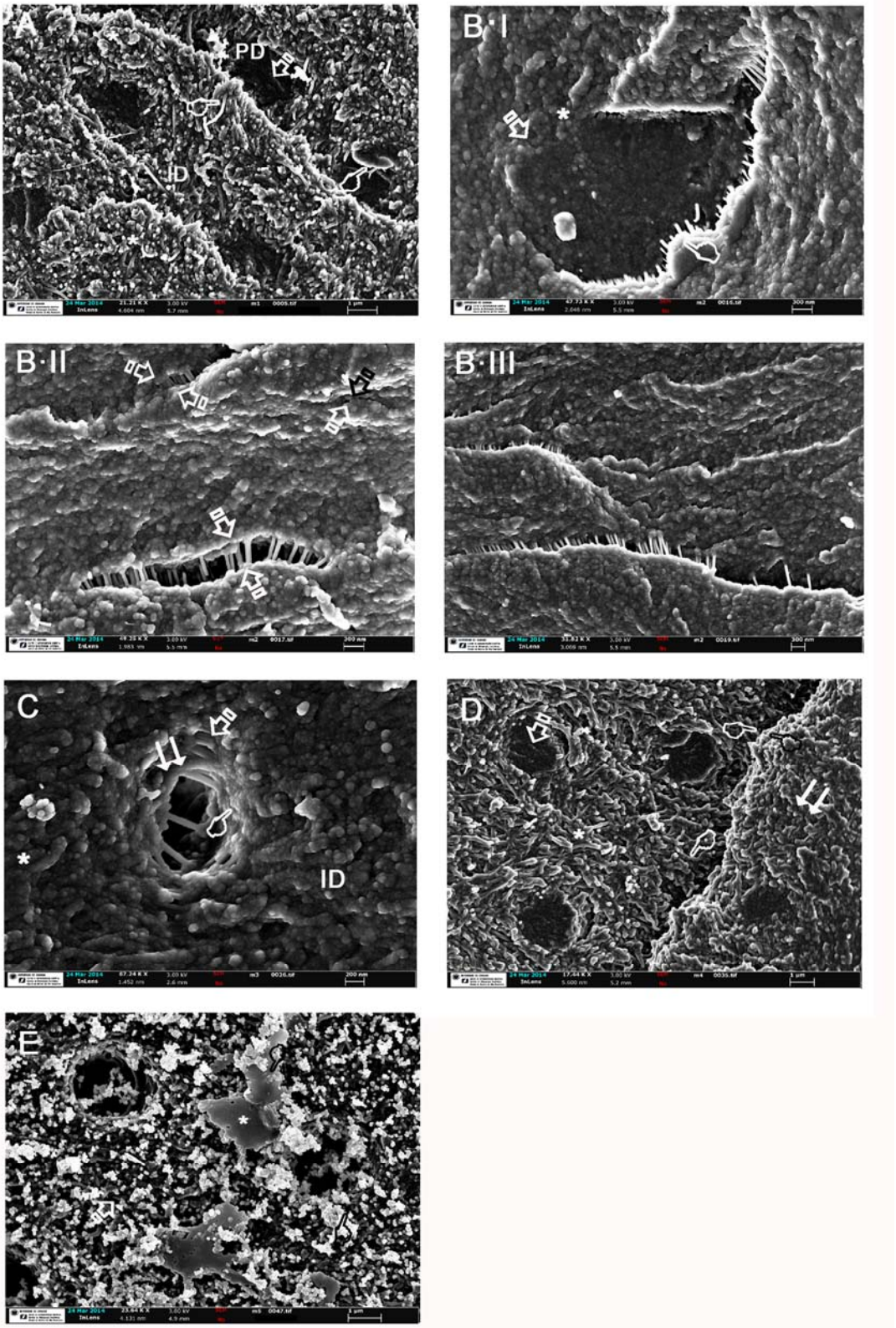

FIGURE 3/1

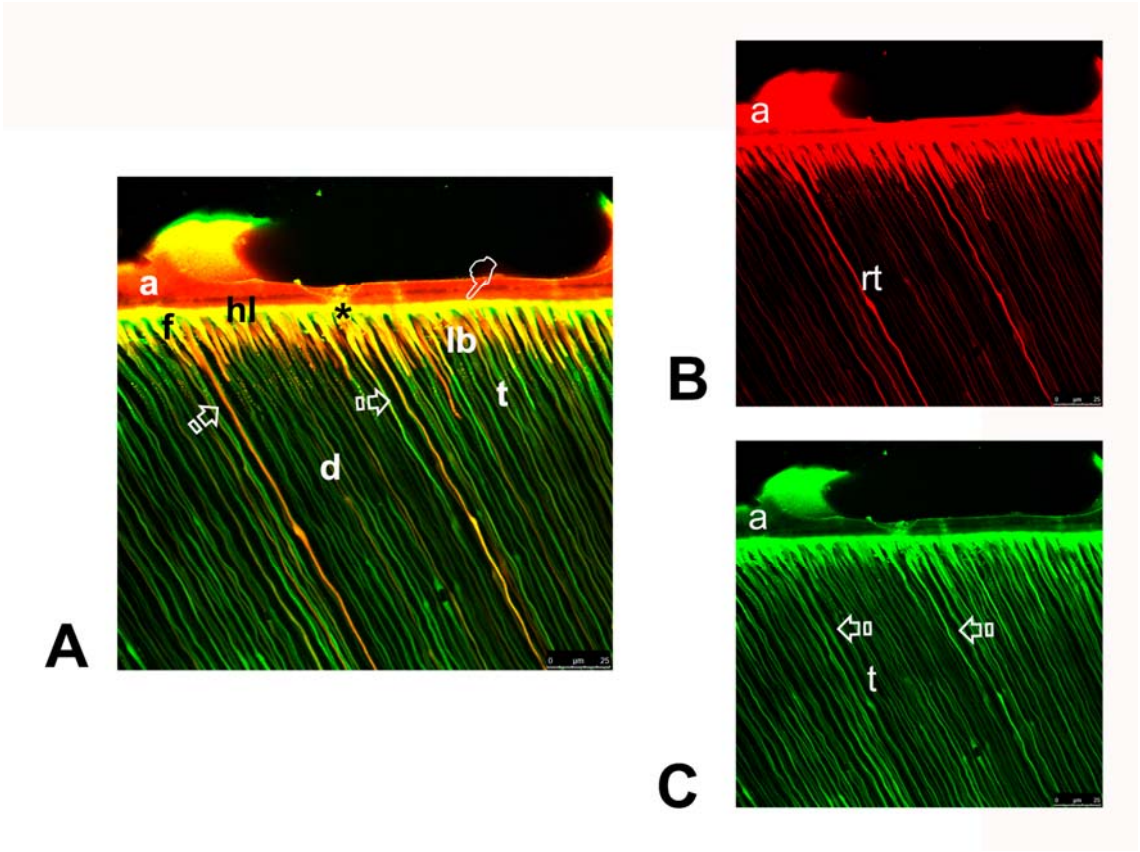

FIGURE 3/2•I

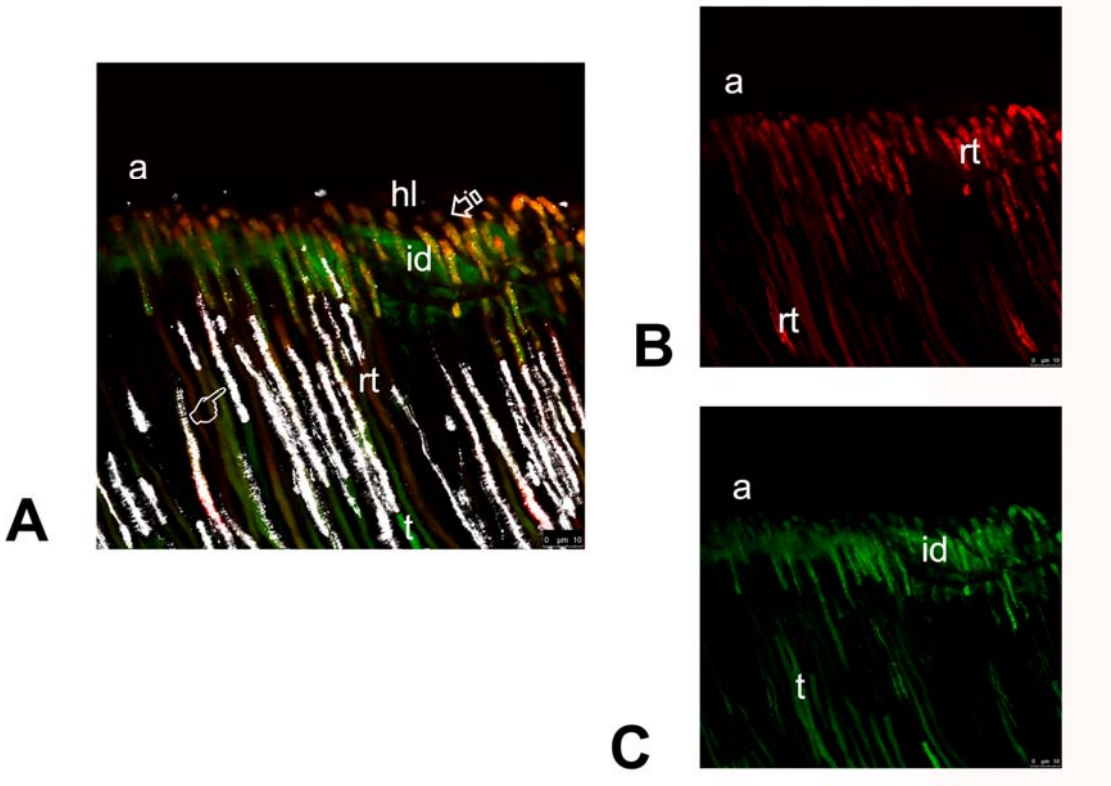

FIGURE 3/2•II

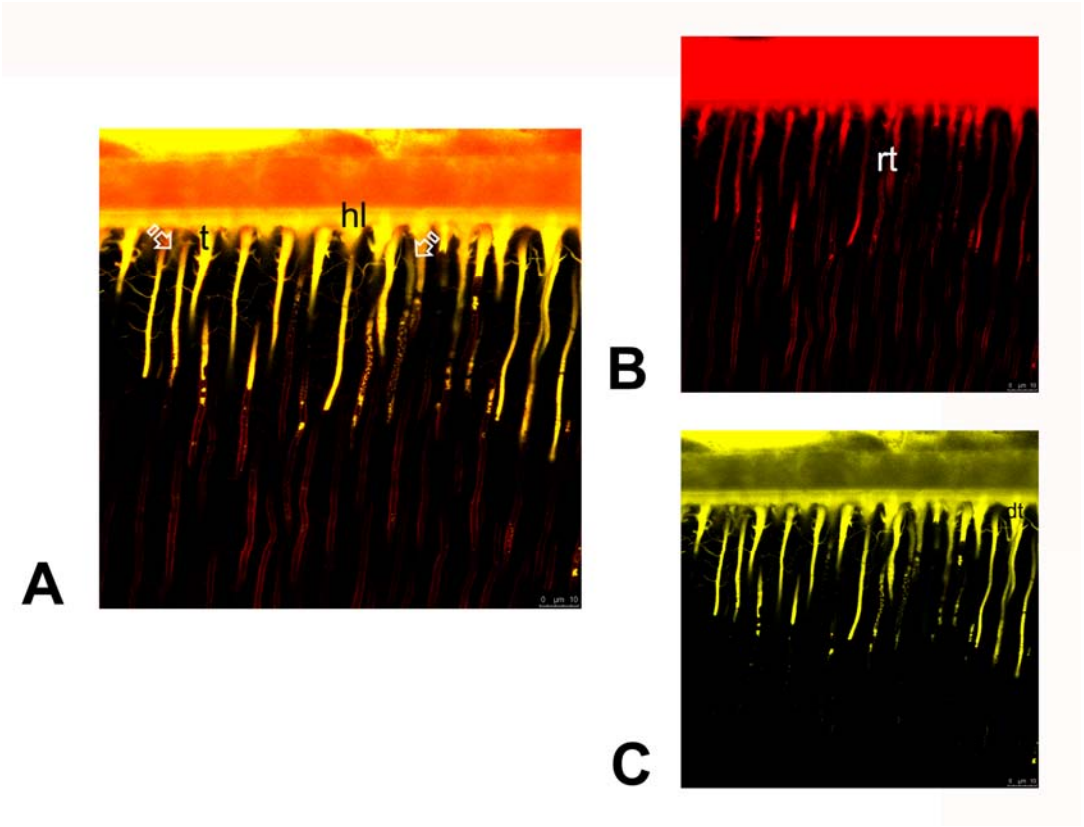

FIGURE 3/3

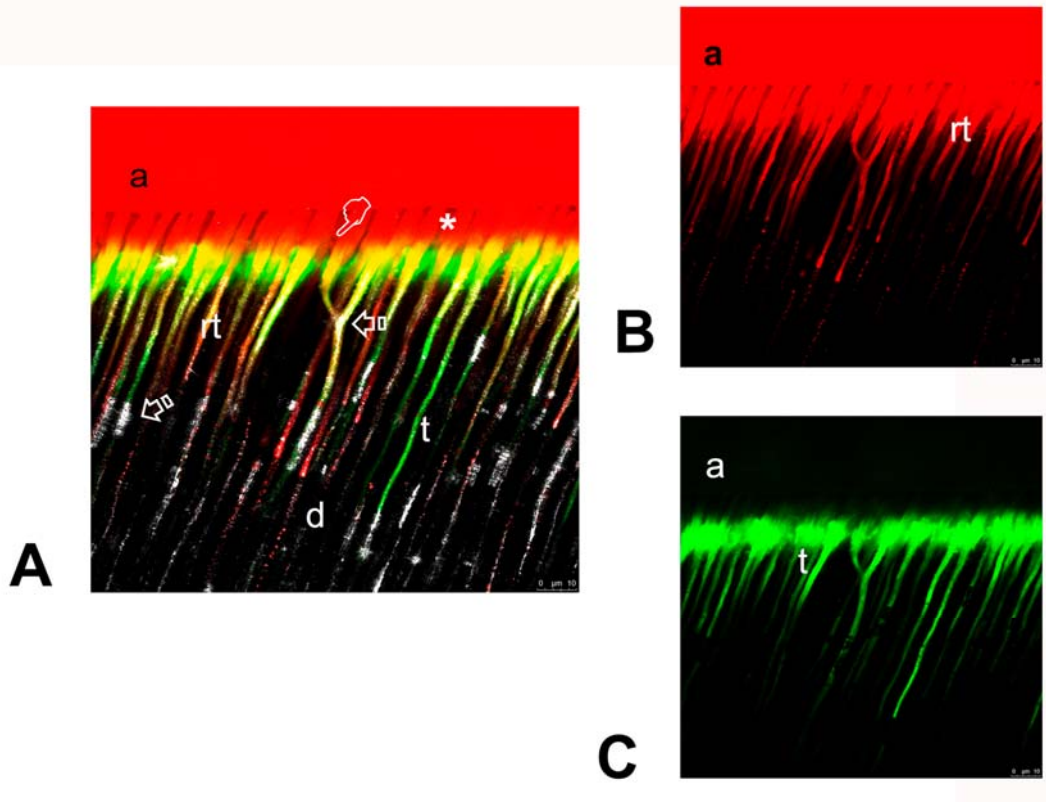

FIGURE 3/4•I

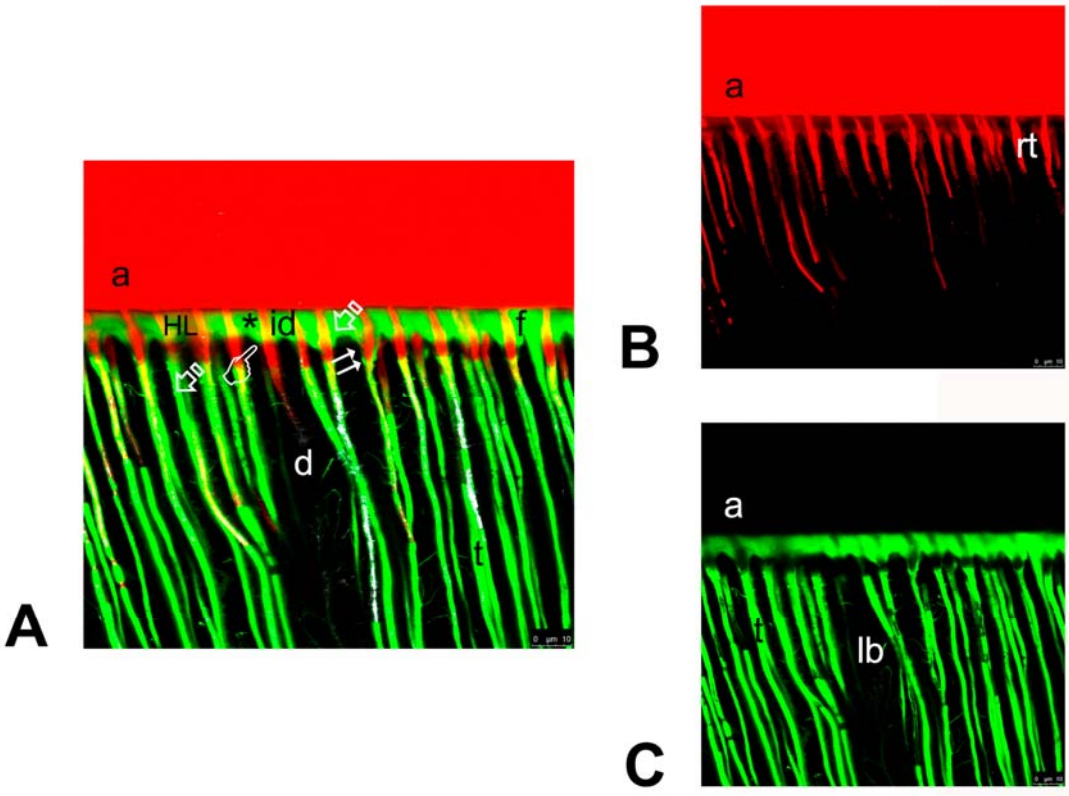

FIGURE 3/4•II

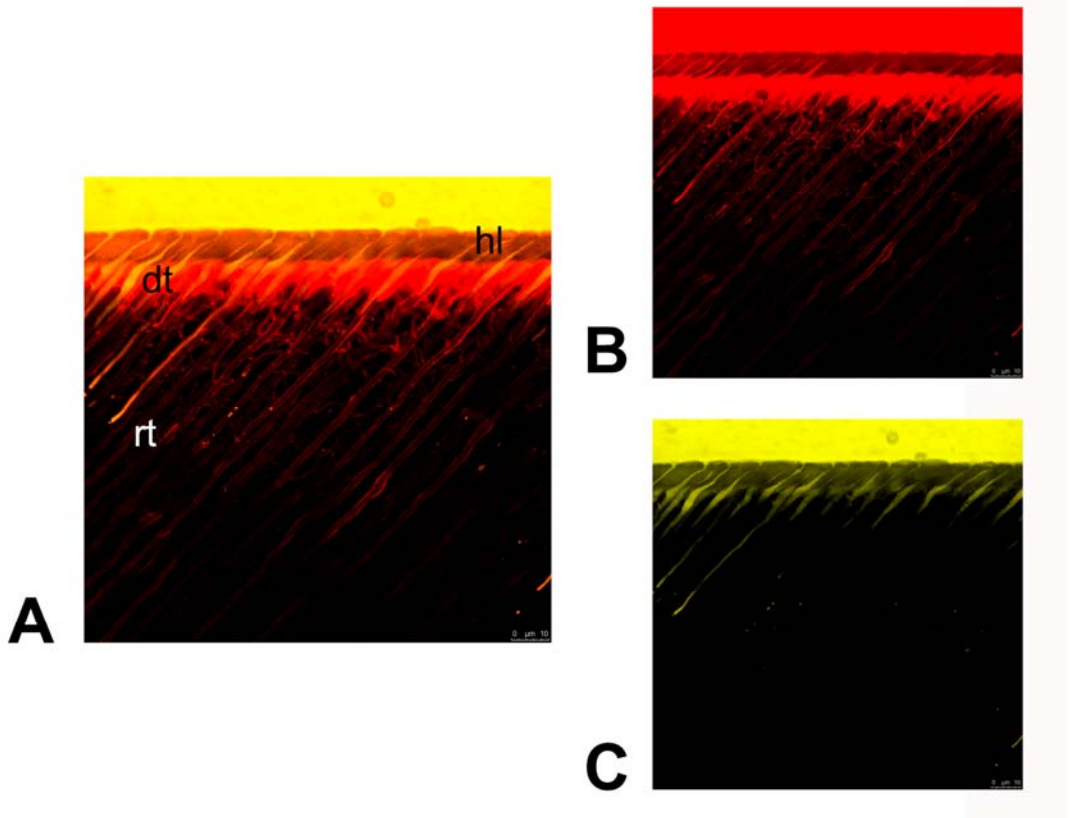

FIGURE 5

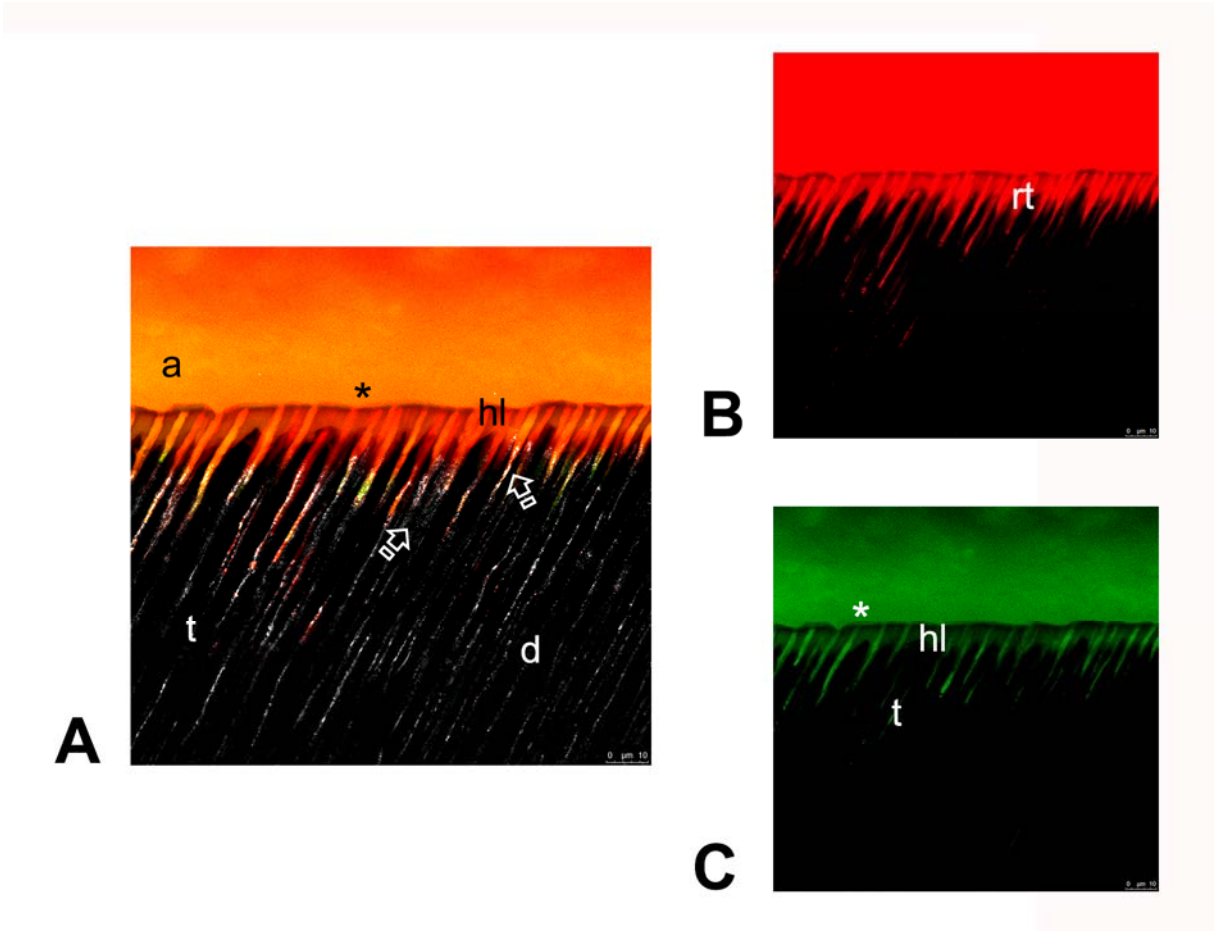

Table 1. Materials used in this study and respective manufacturers, basic formulation and mode of application.

Product details	Basic formulation	Mode of application
Adper Single Bond Plus (SB) (3M ESPE, St Paul, MN, USA)	Bis-GMA HEMA dimethacrylates ethanol water a novel photoinitiator system a methacrylate functional copolymer of polyacrylic polyitaconic acids	**Dentine conditioning** 37% H_3PO_4 (15 s) **Adhesive application** Rinse with water Adhesive application (30 s) Light activation (15 s)
Phosphoric acid 37% (Braun Medical SA, Barcelona, Spain).		
X-FlowTM (Dentsply, Caulk, UK)	Strontium alumino sodium fluorophosphorsilicate glass, di- and multifunctional acrylate and methacrylate resins, DGDMA, highly dispersed silicon dioxide UV stabilizer, ethyl-4-dimethylaminobenzoate camphorquinone, BHT, iron pigments, titanium dioxide	

Abbreviations: Bis-GMA: bisphenol A diglycidyl methacrylate; HEMA: 2-hydroxyethyl methacrylate; DGDMA: diethyleneglycol dimethacrylate phosphate; BHT: butylated hydroxytoluene; H_3PO_4: phosphoric acid; UV: Ultraviolet.

Table 2. Mean and standard deviation of microtensile bond strength values (MTBS), in MPa, and percentage distribution (%) of failure mode (A: Adhesive; M: Mixed), obtained for the different experimental groups.

	Mean (SD) MPa	Failure mode	
		A %	M %
PA+SB Unloaded	34.7 (8.55)	30	70
PA+SB Sine	26.5 (5.57)	45	55
PA+SB Square	20.1 (5.91)	52	48
PA+SB Hold 24h	26.9 (8.53)	44	56
PA+SB Hold 72h	25.4 (4.81)	48	52

Significant differences were not obtained.

Abbreviations: PA: phosphoric acid; SB: Single-Bond.

Table 3. Means and SD of dynamic viscoelastic moduli: complex modulus (E*) and storage modulus (E´) (GPa) of the hybrid layer (HL), bottom of hybrid layer (BHL), peritubular (PD) and intertubular dentine (ID) at the experimental interfaces. Rows with different letters are significantly different (P<0,05).

	variables	24h X (SD)	Sine X (SD)	Square X (SD)	Hold 24 h X (SD)	Hold 72 h X (SD)
HL	**E***	3.65 (0.17)a	3.50 (0.07)a	3.12 (0.14)b	5.53 (0.22)c	3.19 (0.21)b
	E'	3.60 (0.25)a	3.45 (0.20)a	1.90 (0.12)b	5.11 (0.33)c	2.37 (0.26)d
BHL	**E***	4.2 (0.27)a	4.78 (0.25)b	4.93 (0.29)b	10.96 (0.34)c	4.85 (0.17)b
	E'	1.20 (0.26)a	0.72 (0.11)b	0.66 (0.29)b	1.84 (0.25)c	1.27 (0.48)a
PD	**E***	25.00 (0.67)a	57.30 (0.55)b	58.95 (8.04)b	68.45 (11.03)b	59.51 (10.78)b
	E'	24.00 (0.31)a	22.41 (0.73)b	19.65 (1.85)b	26.28 (3.04)c	35.71 (1.79)d
ID	**E***	17.00 (0.27)a	50.01 (0.47)b	49.7 (0.58)b	80.62 (2.21)c	56.91 (0.62)d
	E'	16.00 (0.48)a	17.93 (0.52)b	17.26 (0.37)b	16.58 (0.54)a	35.50 (0.57)c